Mata, D.; Scharnagl, N.; Lamaka, S.V.; Malheiro, E.; Maia, F.; Zheludkevich, M.L.:
Validating the early corrosion sensing functionality in poly (ether imide) coatings for enhanced protection of magnesium alloy AZ31.
In: Corrosion Science. Vol. 140 (2018) 307 - 320.
First published online by Elsevier: 31.05.2018

DOI: 10.1016/j.corsci.2018.05.034
https://dx.doi.org/10.1016/j.corsci.2018.05.034

Validating the early corrosion sensing functionality in poly (ether imide) coatings for enhanced protection of magnesium alloy AZ31

D. Mata[a], N. Scharnagl[b]*, S.V. Lamaka[b], E. Malheiro[a], F. Maia[a], M.L. Zheludkevich[b,c]

[a]Smallmatek - Small Materials and Technologies, Rua dos Canhas, 3810-075 Aveiro, Portugal

[b]Institute of Materials Research, Helmholtz-Zentrum Geesthacht, Max-Planck-Straβe 1, 21502 Geesthacht, Germany. E-mail: nico.scharnagl@hzg.de

[c]Faculty of Engineering, Christian-Albrechts-University of Kiel, Kaiserstr. 2, D-24143 Kiel, Germany

Graphical abstract

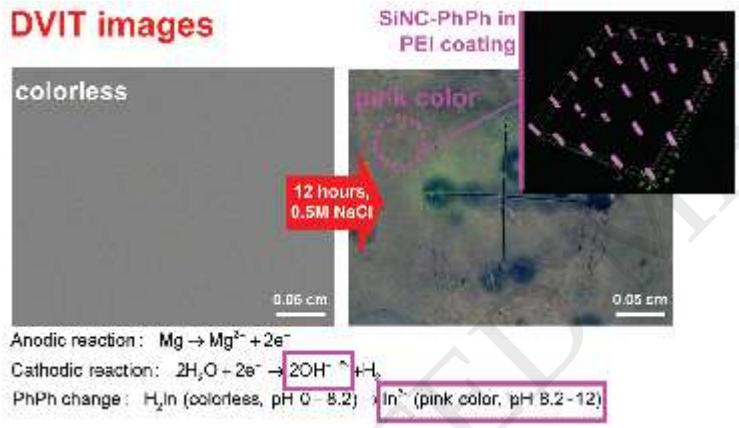

Highlights

- Bifunctional coating is proposed to enhance the service life of corrosion susceptible AZ31 alloy
- The pH changes following corrosion outbreak trigger both corrosion sensing and self-healing functionalities
- Observations evidence correlation between kinetics of color signaling and corrosion activity

Abstract

This work reports on the validation studies of early corrosion sensing poly ether imide (PEI) coatings with incorporated pH-sensing phenolphthalein loaded silica nano-sized capsules (SiNCs-PhPh) on AZ31 magnesium alloys. Immersion and drop tests validated the high sensing accuracy and PhPh color-signaling reproducibility of the coatings upon onset of corrosion. This behavior is correlated to the homogeneous dispersion of SiNC particle agglomerates confirmed by 3D Raman mapping and SEM analysis. Complementary differential video imaging technique (DVIT) assisted by electrochemical impedance spectroscopy (EIS) investigations provided clues for a good correlation between the kinetics of color signaling and the corrosion activity. Mechanistic insights into the pH-sensing/color-signaling functionality in PEI coatings are suggested.

Keywords: Magnesium, polymer coatings, EIS, Raman spectroscopy

1. Introduction

Magnesium and its alloys have emerged as advanced engineering materials with remarkable properties, triggering a rush for countless applications. Beyond their widely reported properties, such as high strength-to-weight ratio [1, 2], their top listed shortcoming has always been the low corrosion resistance [1, 2], which has hindered their structural applications across a broad range of industrial sectors.

On the way to find suitable corrosion protection systems for magnesium alloys, great efforts have been made in the last decades, whereby some successful engineering solutions have already been applied [3-5]. Various approaches were used to face the challenging intrinsic micro-galvanically stimulated corrosion in impure magnesium or common magnesium alloys. Alloying magnesium with rare-earth elements [6] to reduce

the potential of galvanic coupling, or chemical etching of the alloy surface to reduce the presence of non-alloying elements like Fe, Cu or Ni and other contaminants [7, 8], are just a few examples of approaches commonly applied. To pursue a more general approach to combat corrosion in magnesium alloys, efforts have been made towards finding suitable coatings, in which plating, conversion coatings [9] and organic coatings are included [3-5, 10-12]. These acts as electrical, physical or physico-chemical barriers between magnesium or other metals (galvanic-coupling) and the corrosive environment [3-5, 12]. The most industrial relevant polymeric coatings for magnesium alloys are polyacrylates, polyurethanes, polyesters, polypyrroles and epoxies [3], among the latest sol-gel coating technology [13], mostly silanes. Other sol-gel coatings compositions have been developed as well, but are still in the maturation phase, such as hybrid organic-inorganic silanes [4], including epoxy-based [10-12, 14]. Overall, they represent a set of technical requisites to enhance corrosion protection, namely, high thermal and mechanical resistivity, high chemical stability, low water vapor and ion permeability, as well as an important outstanding adhesion [14, 15]. However, under the harshest working conditions, especially in Cl^- containing environments, most of the polymeric systems partially fail to prevent the ingress of Cl^-. Ultimately, this leads to the onset of corrosion of magnesium and the destruction of the native $Mg(OH)_2$ protective layer. These events set localized alkaline conditions alongside with the precipitation of $Mg(OH)_2$ products at large extent [12, 16, 17], which when combined, compromise the adhesion of the coating and, as a result, the loss of its primary corrosion protection.

Encouraging results on investigating other class of polymers, better suitable to protect magnesium against corrosion, have been found under the study of promising poly (ether imides) (PEI) with self-healing properties [15, 18-22]. Important milestones were accomplished in the last years, briefly: (1) optimized pre-treating procedures for AZ31 magnesium alloy have significantly enhanced the adhesion of PEI and other coating

materials to this metal, and subsequently its corrosion protection [8]. (2) Under proper selection of the solvent system, porous or dense coatings can be prepared, each one with its own key advantages towards corrosion protection [15, 18]. Coatings with a solution of PEI dissolved in N,N'-dimethylacetamide (DMAc) are based on a phase inversion process where the polymer precipitates in the presence of humidity from air and builds a microporous layer (pore size approx. <0.5 µm). Changing the solvent system for the polymer solution to solvents with lower vapor pressure and higher polarity like dichloromethane (CH_2Cl_2, DCM) it will also change the phase inversion. The resulting polymer layer becomes dense, transparent and mostly free of defects [23, 24]. While the porous coatings have a lower barrier property due to their porosity, which is related to efficient release of hydrogen while maintaining the integrity and adhesion of the coating, the dense coatings have higher impedance values than the porous counterpart, in the range of 10^8-10^9 Ohm.cm^2 [15, 19-21]. This corresponds to the performance of typical effective coatings systems with barrier properties for corrosion protection purposes [3]. (3) PEI was recognized as a polymer with self-healing capability in strong alkaline environments due to the presence of aromatic imide rings which are able to chemically bond to the $Mg(OH)_2$ surface, in a defect location, via Lewis acid–base interactions towards hydroxamic acid anions [15, 18]. This self-healing mechanism expects an extension of the service-life of AZ31 magnesium alloy in corrosive environments [15, 18, 20-22]. Unfortunately, this healing capability might get lost if the initial defect becomes too large for the polymer to fill it completely [15].

As further improvement for these PEI coatings, it is proposed a complementary corrosion sensing system which is able to spot corrosion events and make them detectable by visual inspection. Timely detection of corrosion prevents its general propagation and allows fast repair of the damaged part, which in turn saves high costs in

maintenance. This is particularly envisaged for magnesium alloys, since they are known for their extremely high corrosion susceptibility.

pH-sensing systems based on phenolphthalein (PhPh) pH-indicator, including silica nanocapsules containing PhPh (SiNC-PhPh) ones [25], have been proven to be highly efficient to early detect corrosion events [25-28]. The use of a host-capsule material for PhPh improves the service-life of the sensing functionality. The PhPh is encapsulated in the SiNCs and is kept entrapped while its color is changed under service conditions. This allows the preservation of color-signal intensity and the use of this sensor particle under multiple demands, making possible a longer lasting of its functionality [25-28]. Upon onset of corrosion, the hydroxide anions (OH^-) formed at the cathodic site change color of otherwise colorless PhPh indicator to strong pink-color within the range of pH 8.2 – 12. This indication can then easily reveal the active sites for visual inspection [25]. Most of the studies validate the corrosion sensing mediated by PhPh on coating systems that are chemically stable at alkaline conditions [25, 26]. Therefore, the polymer neither consumes OH^-, nor interferes with the change of color of PhPh. On the other hand, when using PEI polymer with self-healing behavior activated by alkaline environment caused by existence of OH^- [15, 18], it becomes necessary to validate the efficiency of the PhPh sensing mechanism.

This work focuses on optimization of a new multi-functional protective coating presenting a synergistic self-healing and corrosion sensing performance. The validation studies of the pH-sensing/color-signaling functionality of SiNC-PhPh containing PEI coatings on AZ31 magnesium alloy substrates are reported. Here, the pH-sensing corresponds to the functionality of the PhPh indicator to sense corrosion via a change of color, while color-signaling corresponds to the easiness of PhPh pink color visualization on the coating under service. The influence of the distribution and the amount of SiNC-PhPh sensor particles in the polymer matrix on the success of color detection on large areas is

thoroughly discussed. The influence of the porosity of the PEI coatings was investigated, as well. High efficient pH-sensing/color-signaling systems able to detect even the smallest corrosion events at micron size range, which are out of the detection range of the EIS testing, are presented and the respective mechanism is discussed.

2. Material and Methods

2.1 Reagents and materials

All chemicals used are of analytical grade: dichloromethane (DCM, ≥99.8%, Merck), N,N'-dimethylacetamide (DMAc, ≥99.8%, Merck), poly(ether imide) polymer (PEI, Ultem® 1000, General Electric), phenolphthalein (PhPh) loaded silica nano-sized capsules (SiNC-PhPh, ADDPRIME®, Smallmatek).

Metal substrates of AZ31 magnesium alloy with the following composition (wt. %) were used: Al 2.970%, Zn 0.845%, Mn 0.236%, Si 0.0226%, Cu 0.002%, Ca 0.003%, Ni 0.004%, Fe 0.026%, balance Mg.

2.2. Preparation of SiNC-PhPh/PEI formulations

SiNC-PhPh nanosensor particles with diameter size in the range of 100 - 150 nm were prepared via an oil-in-water microemulsion, as described previously elsewhere [25]. Prior to their use in PEI formulations, SiNC-PhPh were vacuum dried at 40 ºC and 10 mbar overnight. The SiNC-PhPh/PEI formulations in DMAc (10 wt.% PEI for porous films) were prepared by three main protocols (Table 1), at a fixed weight ratio of SiNC-PhPh/PEI of 1:20 (5 wt.% related to PEI), to evaluate the dispersibility of the particles in the PEI matrix. In protocol 1, dried SiNC-PhPh powders were added directly to PEI solution and

then stirred at 800 rpm for 1 h. For protocols 2 and 3, two steps were used. The SiNC-PhPh powders were firstly pre-dispersed in the DMAc at different conditions: 650 rpm/1 h (protocol 2) and 500 rpm/5 h (protocol 3). Afterwards, the SiNC-PhPh suspensions were added drop-wise to the PEI/DMAc solutions while stirred and left to stir under two established conditions: 800 rpm/1 h (protocol 2) and 300 rpm/24 h (protocol 3). All protocols were carried out at room temperature.

2.3. Preparation of free-standing films and dip coated SiNC-PhPh/PEI coatings

For quick evaluation of the dispersibility and compatibility of SiNC-PhPh particles with PEI, free-standing films were prepared on pre-cleaned glass substrates using a casting blade of 120 µm of wet film thickness. PEI films were prepared with DMAc solvent to form porous films which could be easily detached from the glass substrate. Two sets of PEI films were prepared, one highly porous with white appearance, dried at room temperature overnight, and one transparent with lower porosity, vacuum dried at 60 ºC and 10 mbar overnight. The resulted free-standing dried PEI films have an average thickness of 7 µm with a good mechanical resistance to be easily handled.

The SiNC-PhPh content in the PEI formulations were varied (0.5, 1, 2, 5 and 10 wt.% related to PEI) to asses the pH-sensing/color-signaling functionality of the coatings systems (Table 1).

Before the preparation of dip coated PEI coatings, the AZ31 substrates (5 x 2 cm^2) were pre-cleaned in acetic acid (100 g/L + 50 g $Ca(NO_3)_2$) for 1 min to reduce galvanic cell inducing Fe and Ni intermetallics, following an optimized protocol previously reported [8]. Both porous and dense PEI coatings were prepared with DMAc (10 wt.% PEI in DMAc) and DCM (8 wt.% PEI in DCM) solvents, respectively. Dip coated samples were obtained by dipping the metal substrates in PEI formulations for 1 min, following a resting period of

3 min at room conditions, and finally, a second dip for 10 s [15]. All dip coated samples were dried at room temperature overnight.

2.4. Characterization techniques

Scanning electron microscopy (SEM, Tescan Vega3 SB) operated at an acceleration voltage of 8 kV with a working distance of 6 mm was used to examine in planar-view the morphology of samples. Before the SEM analysis, all polymeric coating samples were pre-sputtered with a conductive gold layer to reduce charge effects onto the surface. The equipment is coupled with an energy dispersive X-ray (EDX) detector to perform elemental distribution analyses of the Si Kα-shell signal of the SiNC-PhPh. These 2D maps were collected at 8 kV with a working distance of 15 mm, dwell time of 10 s and resolution of 512 scans. After adjusting contrast and threshold levels of the EDX images (RGB color format) using the Image J software (v1.46r), the SiNC-PhPh particles were analyzed in size and area with the measuring tools available in the software. The output files in ASCII format were then imported into OriginPro 8 (v8.0724) software to prepare the respective particle size distribution histogram plots.

The fraction area of the SiNC-PhPh particles was obtained, as follows

$$\%\ Fraction\ area\ of\ SiNC-PhPh = \frac{A_{total\ SiNC-PhPh}}{A_{total}} \times 100, \quad (1)$$

where $A_{SiNC\text{-}PhPh}$ is the total area of SiNCs-PhPh particle agglomerates and A_{total} is the total area of the 2D image.

Optical microscopy (Leica DC 300 stereomicroscope) was used to investigate the pH-sensing/color-signaling functionality of the prepared systems, including the distribution homogeneity of the PhPh pink color in the PEI coatings after exposure to alkaline conditions.

Confocal Raman spectroscopy (Bruker, Senterra) was applied to perform 3D mapping analysis of the final coatings to evaluate the distribution of the SiNC-PhPh particle agglomerates in the PEI matrix. The acquisition of data in depth mode was performed giving a total analyzed volume of 100×100×10 μm^3. All spectra were collected with an excitation wavelength of 532 nm, laser power of 5 mW, aperture of 25 µm and 256 scans for an appropriate signal-to-noise ratio, with an integration time of 2s. The distance between two neighbor points in the 2D matrix was of 25 µm (ΔX=ΔY=100 µm), and a total number of 6 slices with a ΔZ of 2 µm were acquired.

The % signal of SiNC-PhPh was calculated, as follows

$$\%\ SiNC-PhPh = 100 - \frac{\left(\frac{I_{1384}-I_{1415}}{I_{1384}}\right) - \left(\frac{I_{1384}-I_{1415}}{I_{1384}}\right)_{MIN}}{\left(\frac{I_{1384}-I_{1415}}{I_{1384}}\right)_{MAX} - \left(\frac{I_{1384}-I_{1415}}{I_{1384}}\right)_{MIN}} \times 100, \quad (2)$$

where $I_{1384cm\text{-}1}$ and $I_{1415\ cm\text{-}1}$ are the intensities of the Raman shifts assigned to PEI and SiNC-PhPh, respectively [29, 30]. Here, a value of 0% means that no SiNC-PhPh signal was detected, and 100% indicates a positive detection. Data were extracted from the Bruker OPUS (v7.5) software as ASCII format files and imported into OriginPro 8 (v8.0724) software for further data preparation, including the 2D slice images mapping the positions of the SiNC-PhPh particle agglomerates. The final stacking of the 2D slices images to form a 3D reconstruction was done with the Image J software (v1.46r) using the plug-in 3D Viewer (v10.09.2012).

The volume of SiNC-PhPh particle agglomerates in the 3D reconstruction was calculated, as follows

$$\%\ Volume\ of\ SiNC-PhPh = \frac{V_{total\ SiNC-PhPh}}{V_{total}} = \frac{\left(\frac{A_i\left(\alpha \times 0.25 + \beta \times 0.5 + \lambda\right)}{2 \times A_{SiNC-PhPh}} \times V_{SiNC-PhPh} \right)}{V_{total}} \times 100, \quad (3)$$

where A_i is the expected intersection area of two neighbor points measured with an aperture size of 25 µm, α is the number of pink color points at the corners of the 3D reconstruction, β is the number of pink color points at the edges, λ is the number of pink color points in the volume, 0.25 and 0.5 are corrector factors regarding the corners and edges limitations in the 3D reconstruction, respectively, a pink point in the 3D reconstruction corresponds to a fixed number of SiNCs-PhPh agglomerates of 1.3 µm in diameter (average size for dense coatings, see section 3.2) that can be confined in the area of A_i, $A_{SiNC\text{-}PhPh}$ is the area of one SiNCs-PhPh particle agglomerate of 1.3 µm, $V_{SiNC\text{-}PhPh}$ is the respective volume of one SiNCs-PhPh particle agglomerate and V_{total} is the total analyzed volume of 100×100×10 µm^3 (i.e volume of the 3D reconstruction).

Drop tests and immersion tests with NaOH and NaCl aqueous solutions were conducted to fast check the pH-sensing/color-signaling functionality of the SiNC-PhPh particles. Cyclic drop tests were performed with free-standing films. In a typical cycle, a drop of 0.05 M NaOH (50 µL, pH 12.7) was placed onto the film for up to 5 min until the appearance of the PhPh pink color was observed. Afterwards, the sample was rinsed with deionized water until fully recover its initial colorless aspect. Finally, the sample was dried at room temperature. Two more cycles were repeated consecutively, with a waiting period between cycles of 3 days, to evaluate the reproducibility of the signaling system. For the immersion tests, the coated samples were kept immersed in 0.5 M NaCl (pH ≈ 7) up to 3 days. Photographic record of the color changes of solutions and samples was done at different inspection times. All tests were performed at room temperature.

Electrochemical impedance spectroscopy (EIS) was performed at room temperature using a three-electrode cell assembly with a platinum electrode as the counter electrode, coated AZ31 sample as the working electrode (exposed area of 0.5 cm^2) and a Ag/AgCl electrode as the reference. An aqueous solution of 0.5 M NaCl (350 mL) was used as the electrolyte. To avoid the interference from external electromagnetic fields, all tests were performed inside a Faraday cage. Room temperature measurements were done using a Gamry Reference 600 potentiostat/galvanostat/ZRA at different immersion times up to 3 weeks. A frequency range from 10^5 to 10^{-2} Hz, with a sinusoidal perturbation of 10 mV rms vs. open circuit potential (OCP), with 9 points per frequency decade was used. Two replicates were acquired to check minimum reproducibility. Within good agreement between replicates, representative plots of each system were presented only.

For continuous recording measurements of corrosion activity and color visualization on the surface of the sample, a set-up combining EIS and the difference viewer imaging technique (DVIT) [31] was used. Coated substrates (10 x 10 mm^2) were mounted in an epoxy resin for an easier handling. An exposing window area of 3 x 3 mm^2 on the surface of the sample was prepared with an isolating wax frame. EIS was acquired at fixed frequency of 10^{-2} Hz, giving information about corrosion activities of the complete protective coating scheme. A sinusoidal perturbation of 10 mV rms vs. OCP was applied. EIS data were continuously recorded every 5 min, up to 4 days of immersion in 0.5 M NaCl solution (10 mL), alongside with a photograph acquisition of the surface at the same time frequency. To evaluate the corrosion signaling on a defected surface, an artificial defect was sculpted (two scribes of 1.5 mm in length perpendicularly positioned to each other) and the color mapping was monitored by DVIT (magnification of 1.5X) up to 12 h of immersion. All tests were carried out at room temperature. Two samples of each system were tested to confirm minimum reproducibility.

3. Results and discussion

3.1. Optimizing SiNC-PhPh/PEI formulations with pH-sensing/color-signaling functionality

Fig. 1 presents a set of SEM and respective EDX mapping images of the SiNC-PhPh/PEI free-standing films prepared on glass substrates by three different protocols (Table 1) at fixed SiNC-PhPh loading content of 5 wt.%. The mapping of the Si signal gives an indication of the distribution of the SiNC-PhPh particles (Figs 1b, e and h). Taking into account the average particle size values presented in the histogram plots (Figs. 1c, f and j), it can be attested that no significant differences in particle size are seen across the samples. Nevertheless, it becomes evident that protocol 3 yields the most homogeneous particle size distribution among the other two, being the only one with a single distribution peak at 2.9 μm fitted by a Gauss curve (inset plot of Fig. 1j). Additionally, the superior performance of protocol 3 is supported by the presence of particle agglomerates below 1 μm.

Further studies with protocol 3 were conducted. The SiNC-PhPh content of the coatings was varied in the range of 0.5 - 10 wt.% (Fig. 2) to find the threshold content to obtain coatings with adequate pH-signaling properties under alkaline conditions. In other words, find the minimum amount of SiNC-PhPh in the coating to obtain a detectable PhPh pink color change for visual inspection. To evaluate this, drop tests with 0.05 M NaOH on SiNC-PhPh/PEI free-standing films were performed. From the photographs, it is evident that the SiNC-PhPh content threshold is 2 wt.% with a strong pink color observed (Fig. 2h), but to seek for an easier detection, the 5 wt.% composition was selected as the optimal one (Fig. 2j). The higher intensity and uniformity of color on the surface of the 5 wt.% composition, compared to the 2 wt%, is not only due to the higher amount of PhPh in the

coating, but it might be also related to the homogeneous distribution of the particle agglomerates in the polymeric matrix (Figs. 2g and 2i), yielding increased surface area.

The statistical data of Fig. 3 show that the increasing content of SiNC-PhPh promotes an increase of the particle size, but not significantly, with all compositions having an average particle size of 3 μm. It must be also highlighted that the surface analyses give good information about the homogeneous distribution of the particle agglomerates in volume. This is assumed because Fig. 3a shows the fraction area values (eq. 1) of the particle agglomerates very close to the values of the particle content in volume. The vol.% was directly calculated from the wt.%.

The drop tests of Fig. 4a give some insights in the kinetics of the PhPh color change for the 5 wt.% composition. After one drop of 0.05 M NaOH (50 μL, pH 12.7) was placed on top of the SiNC-PhPh/PEI sample, their coloration was recorded over time. After 5 s, the color starts to appear, and right after 5 min, the color reaches the maximum of intensity. Cyclic drop tests of NaOH exposition (Fig. 4b) proved that the signaling properties were kept almost intact after 3 cycles. The preservation of color after multiple cycles indicates that the PhPh kept stored inside the SiNC-PhPh. Nevertheless, there was some diffusion of PhPh out of the SiNC-PhPh because the drop color was turned to pink. These results anticipate a good performance of the pH-sensing/color-signaling functionality in more realistic applications, since the drop tests simulates conditions of atmospheric condensation, in which coatings are exposed to thin films or drops of electrolyte [32]. In these tests the fully immersion is excluded, and there is a restriction of the diffusion mechanisms [32].

3.2. pH-sensing/color-signaling functionality of SiNC-PhPh/PEI coatings on AZ31 substrates

To understand the effect of opacity and density of the polymer on the pH-sensing/color-signaling functionality of SiNC-PhPh/PEI coatings on AZ31 substrates, two different coating samples were prepared. While the dispersing process used to prepare the samples was equal, the solvents applied cause different film forming processes for PEI [15, 18, 20-22]. The first one prepared with DMAc is a phase-inversion process that leads to white colored (Fig. 5a) highly rough (Figs. 5b and 5c) and porous films (pore size < 0.5 µm) [23], while the second prepared with DCM, based on solvent evaporation, is a dense and transparent (Fig. 5f) film [24] (Figs. 5g and 5h) [15, 18, 20-22]. The porous and dense films formed on AZ31 substrates have dry thicknesses of 40 µm and 70 µm, respectively (Figs. 5b and 5g).

The EDX maps and respective histograms of the particle distribution of the samples are presented in Figs. 5d-j. The results show that the SiNC-PhPh diameter size is lower for the dense samples than in the porous one, respectively 1.3 µm and 2.2 µm. Additionally, the particles have better size distribution for the former ones. The Hansen solubility parameters of DCM and DMAc are different having effect on the dispersion of the particles [33]. Moreover, solvents having different water solubility will have different water uptake during the preparation process, ultimately, influencing the kinetics of the PEI phase-inversion process and the final particle dispersion [15, 18, 20-22]. Besides this, the solvent vapor pressures have even a more important contribution especially by using DCM, since it correlates with the evaporation rate. The vapor pressures at 25 ^{o}C for DCM and DMAc are 57.99 kPa and 9.77 kPa, respectively [34]. Thus, much higher evaporation rate is seen in the DCM over DMAc. This delays the settlement of the SiNC-PhPh and therefore, helps to avoid the formation of big agglomerates for the former.

For a more detailed information about the particle distribution in the polymer matrix, 3D Raman studies were carried out for dense coatings (Fig. 6). Only dense coatings were analyzed due to their higher SiNC-PhPh distribution in the PEI matrix over the porous ones

and higher interest for the final application. Moreover, the higher distribution homogeneity of the formers was also important to make prove the level of applicability of the Raman technique on detecting micro-sized particles in the analyzed volume.

Fig. 6a shows the different spectra for SiNC-PhPh, PEI coating and 5 wt.% SiNC-PhPh/PEI coating. In the latter sample, two measurements were acquired at different positions, one on the SiNC-PhPh and other on PEI alone, without detection of SiNC-PhPh signal. It is evident that when SiNC-PhPh are present, the intensity of the assigned band at 1415 cm^{-1} [29] increases and the band of PEI at 1384 cm^{-1} [30] is overlapped by smoothing and decreasing intensity. By applying eq. 2, it is possible to calculate the intensity (%) of SiNC-PhPh signal. A cut-off value between 0 and 100% was used to determine the detection of SiNC-PhPh signal. This was applied to reduce the contribution of the overestimated SiNC-PhPh signal measured. An amplified SiNC-PhPh signal was needed to keep the high resolution of the measurement necessary to detect micron sized particles. The use of a positive interference of signals, i.e. sum of signals intensities, with a laser aperture of 25 µm, allowed obtaining total signal intensities close to the ones with an aperture of 50 × 1000 μm^2. Amplified SiNC-PhPh signals were achieved by two different experimental configurations, with similar interference intensities observed (data not shown). In the first one, it was considered a full overlapping by measuring two neighbor points in the 2D matrix with a length distance between them half the length size of the laser aperture of 25 µm. For the second, a partial overlapping was used by measuring two neighbor points separated at the same length of the laser aperture. The latter configuration was adopted for all measurements. Although, for an easier mathematical calculation of the intersection area of two neighbor measuring points, A_i (eq. 3), the second configuration was considered.

The data collected in a single 2D matrix of 100×100 μm^2 (Figs. 7a) can be presented as a 2D image, mapping the position of the SiNC-PhPh particle agglomerates

(Figs. 7b) in the specific layer by using the intensity signal values of SiNC-PhPh (see Experimental Section 2.4). The final 3D reconstruction of all stacked 2D slices (100×100×10 μm^3) is shown in Fig. 7c. It gives a clear evidence for a homogeneous distribution of the particle agglomerates in the analyzed volume. It must be noticed that each point highlighted by a pink spot (Fig. 7c) represents several agglomerates because the aperture size of 25 µm is higher than a single particle agglomerate of 1.3 µm (Fig. 5i). Moreover, the calculated volume of SiNC-PhPh in the 3D reconstruction (eq. 3) is 2.2 vol.%, close to the nominal volume of 2.9 vol.%. This conformity validates the adopted analyze method for the distribution evaluation of particles in polymeric matrix volume. Additionally, it should be stressed out that due to the low resolution of the Raman technique (Fig. 7c), the collected data give only a rough prediction about distribution of particles in volume. Though, it has a key relevance for any application considering these sensing coatings and should be considered as complementary data to SEM analyses (Fig. 5). The volume particle distribution data give information about the efficiency of color signaling in regards of intensity and resolution across the coating thickness. This follows the premise that when a defect in the coating is formed and reaches the metal surface, the corrosion starts followed by the pH sensing/color signaling, and all the SiNCs-PhPh particles in the defect, in the total exposed area to the corrosive environment, contribute for the pH sensing/color signaling functionality.

The results of the immersion tests in 0.5 M NaCl (pH ≈ 7) summarized in Fig. 8 put in evidence the importance of the SiNC-PhPh/PEI coatings porosity, opacity and particle distribution on sensing and signaling corrosion of coated AZ31 substrates. The results for the porous and dense coatings (Figs. 8a and 8b) show that after 15 min of immersion, the corrosion of AZ31 starts alongside with local increase of pH, changing the color of PhPh to pink. For the control, PEI alone without SiNCs-PhPh, no changes in color are visible, as expected. The early color observations occurred where large edge areas corroded, due to

the failing of thinner coatings at these areas, and worked as strong releasing sources of PhPh for making the color signaling more visible. This explains the odd fast appearance of color on the dense samples with expectable higher barrier. On the other hand, the early color signaling proves that the porous coatings have poor barrier properties. Moreover, for the porous samples the highly interconnected porosity works as a diffusion channel for PhPh, from the substrate of the metal, where it turns pink, towards the top of the coating into the bulk solution medium. This phenomenon can be easily seen in the porous coatings in early stages of immersion, after 1 h (Fig. 8a), by means of a diffusion process driven by concentration gradients. The dense coatings only show this PhPh bleeding behavior after 3 days (Fig. 8b). This bleeding of PhPh out of the SiNCs to the solution was also seen in the drop tests (Fig. 4), but it not occurs significantly. Under cyclic drop tests of exposure to NaOH solution, the PhPh pink color intensity in the coatings is kept almost constant upon multiple uses proving that the PhPh is preserved active inside the SiNCs (Fig. 4). Even tough, when the PhPh bleeding occurs due to the interconnected porosity it always influence at some extent the signaling efficiency of the coatings, especially for porous samples. It weakens the signaling efficiency due to the lost of PhPh pink color intensity at the metal surface, where corrosion should start and be spotted at first place. The residual PhPh pink color that is released to the bulk solution will not contribute for the corrosion signaling because it is vanished overtime with the acidification of the solution when exposed to a CO_2 rich atmosphere. Moreover, the small remaining amount of PhPh pink color that reaches the coating surface will not contribute for the color signaling either because the color disappears really promptly due to the same acidification referred above. This is observed for wet (Fig. 8a) and dry (Fig. 9a) porous samples. Contrarily, in the dense coatings, very clear pink spots are easily seen for longer time due to a restricted diffusion in the pores (Fig. 9b).

The opacity of the samples also has a great influence on the visibility of the color signal. For opaque coatings, it is difficult to detect the appearance of pink color at the metal/coating interface, where corrosion is taking place. For the samples in this study, the white color of the porous coatings worked satisfactorily as a good white-pink contrast exists (Fig. 9a). In the opposite, for dense samples presenting high transparency, it was easy to detect the color beneath the coating at the metal/coating interface (Fig. 9b).

In Fig. 10, EIS spectra of the coatings at full frequency range were taken to evaluate the corrosion processes at the metal/electrolyte interface and barrier properties of the coating over time. Generally, data show that, as expected, the porous coatings (Fig. 10a) have lower barrier properties than the dense ones (Fig. 10b), corroborating the immersion tests (Figs. 8 and 9). In the case of porous layers, a high frequency (10^5 Hz) relaxation process can be assigned to the response from the polymer film. Similar results were reported previously [19-21]. The low frequency resistance in turn is associated to the total resistance, which includes contribution from the polymer and oxide layers together with a charge transfer resistance. No significant differences can be detected for the bare coating compared to the SiNC-PhPh supplemented one (data not shown).

The sample coated with a dense layer has sufficiently superior impedance values at all frequencies, as expected, even after 24 hours of immersion (Fig. 10b). The reason is that the barrier properties of the layer are remarkably higher. At high frequencies the response if fully dominated by the capacitance of the dielectric barrier layer composed by the PEI coating. At lower frequencies one can observe another overlapping relaxation process which can originate from the oxide layer underneath or the first signs of electrochemical activities at the interface. Despite the diffusivity of the electrolyte, the dense coatings keep their morphology and high impedance values, leading to a superior performance over the porous ones.

Any color change on or in the coating layers was detected in none of the samples, even for the dense ones which should possess easier detection ability. The most plausible reason for this can be attributed to a diffusion of the PhPh pink color in the large volume of electrolyte used. Also, the small surface area exposed contributed to the low concentration of PhPh locally, below the naked eye visibility.

In order to be able to correctly assess the correlation of the kinetics of corrosion events with those of color signaling, further EIS measurements were carried out under more appropriate conditions (Fig. 11). Smaller volumes of 0.5 M NaCl were used and the impedance was measured at fixed frequency of 10^{-2} Hz for a faster recording and to increase the chance for a correlation with the color visualization. Particularly for the porous systems, the time constant responsible for corrosion activities appears at low frequency. To record the color, a DVIT technique was used under constant light conditions inside a chamber. The DVIT gives the advantage for detection of color patterns only, thus, making easier the color visualization. The difference image was obtained by digitally subtracting the reference (initial, at t=0) image from each consecutive image. The processed image reveals only differences between the reference and the consecutive image and eliminates background caused by the visible static features in the unprocessed images. [31]

Figs.11a and 11c show that the color was detected on both samples, after similar immersion times, about 1.5 h. These results are in agreement with the immersion tests (Fig.8 and 9), by proving the similar response time of the samples. Additionally, the EIS measurements of Fig. 10 corroborate the observations of Fig. 11. Both samples show diffusion of the electrolyte after 1h of immersion that is necessary to onset a change in pH for PhPh to change the color. Of relevance, these singular corrosion events could not be detected by EIS (Figs. 11b and 11d). These corrosion events should be signaled by significant variations of the impedance values matching the color events seen at the sample surface. But, in its place, almost steady impedance signals were measured for

both samples. This is explained by the very low impedance values for porous samples and the extremely high impedance values for the dense ones that hamper the detection of small signal variations. While for porous samples the measured impedances correspond to the low resistances of R_{ct} (Fig. 10a), for dense coatings the impedance is assigned to the resistance of the coating (R_{coat}) (Fig. 10b). So, porous coatings failed at the very beginning of the test, limiting further observations of corrosion events, because the impedance signal could not drop more (Fig. 11b). On the other hand, for dense coatings, the high impedances make the small amplitude signals of the color related events to not be detected by lack of resolution. However, it can be seen a decrease of the impedance, but not abrupt variations related to the local corrosion activities (Fig. 11d). This decrease in signal is related to the H_2 bubbling seen at the cathodic sites (Figs. 11c). Nevertheless, it can be said that the DVIT assisted EIS testing gives some clues for a good correlation between the color signaling kinetic and the corrosion activity related one. Moreover, despite the failure of EIS in detecting these corrosion events, they were spotted by a simple change of color. These observations prove that the SiNC-PhPh particle agglomerates are well distributed in the coating and are able to sense almost the full surface area exposed to the corrosive environment. Moreover, the sensing resolution of the system is predicted to be at micro-scale range, defined by the combined high distribution and high density of particles. The size of the particle agglomerates also takes an important role in setting the easiness of the color signaling. For bigger particles, the local intensity of color is higher making easier the detection by visual inspection. The combination of these particle characteristics permits these coatings to act as efficient sensing and signaling systems, able to detect even the smallest corrosion events that EIS technique fails to detect.

3.3. Suggested mechanism for the pH-sensing/color-signaling functionality

To further investigate the distribution of color in the surrounding of an artificial defect, complementary tests were performed for dense 5 wt.% SiNC-PhPh/PEI coatings (Fig. 12). The left-side images (Figs. 12 a,c,e and g) correspond to the original optical images and the right-side images (Figs. 12 b,d,f and h) to the respective DVIT treated ones. With a high metal surface area available at the scribe, fast corrosion events took place followed by appearance of pink color, right after the sample was immersed in the electrolyte (Figs. 12a and 12b). The fast signaling of corrosion is due to the threshold pH at pH 8.2 to turn PhPh to pink color, a high concentration of free OH^- anions is present as magnesium starts immediately to corrode. Free OH^- are available because magnesium hydroxides are stable in the range of pH 8.5 - 11.5 [36] only. After 5 min of immersion, the intensity of color, close to the scribe, reaches its maximum, and the localized high concentration of PhPh allows the easy detection of color both by optical (Fig. 12c) and DVIT (Fig. 12d) images.

With increasing immersion time (Figs. 12c-h), corrosion intensifies all over the surface. The color of PhPh spreads over the full immersed area (Figs. 12c-h). The low intensity of color observed prevents its detection under real optical observations. The decreased color intensity is mostly assigned to a diffusion phenomenon and not to a consumption of OH^- mediated by the self-healing of the PEI polymer [15, 18]. However, the second cause cannot be completely discarded, as it is not possible to estimate to what extent it occurs. As described in [15, 18, 37], the self-healing mechanism of PEI at the metal/coating interface is triggered by hydroxamic acids by means of an opening of the PEI imide ring. These N-containing functional groups have high complexation susceptibility with $Mg(OH)_2$ leading to an effective bonding [38]. The following building up of self-assembled polymer monolayers at the corroded spots occurs upon multiple cyclic reactions like a Mg-polyamate [18, 37], until total covering/healing of the defect. These

hydroxamic acids functional triggers are also stable at the metal/coating interface under alkaline conditions in the range of pH 7.8 - 8.5, accordingly to localized SIET measurements on AZ31 substrates [16]. This means that the self-healing of PEI might interfere, at some extent, with the PhPh color change, typically at pH 8.2. However, in overall, it can be confidently stated that no significant interference of the self-healing is seen in the color appearance. The color spots the cathodic reaction, related to the water reduction, due to a local increase of pH, as follows

$$2H_2O + 2e^- \rightarrow 2OH^- + H_2 \quad (4)$$

Besides the color spotted cathodic sites, other equally cathodic sites not spotted can be also presented alongside with a strong release of H_2 gas bubbles and increased pH [16, 17]. The high local pH at these sites, close to pH 12 [17], turns the pink color of PhPh back to its colorless structure form [25], explaining the absence of color. Also, the H_2 bubbling at these sites could help to disperse the color, making it difficult to be observed.

At the scribe, the dissolution of magnesium element mainly, typical of AZ31 alloys [37], occurs at increasing extent over time (Figs. 12c-h) following the anodic reaction,

$$Mg \rightarrow Mg^{2+} + 2e^- \quad (5)$$

Additionally, the absence of color at the scribe might be related to the slight decrease of pH. Lamaka et al. have shown by localized SIET measurements a decrease of pH to values, as low as pH 5.3 [16], that undergoes during the anodic reaction assigned to the magnesium dissolution and hydrolysis [16], as follows

$$Mg + 2H_2O \rightarrow Mg(OH)_2 + 2H^+ + 2e^- \quad (6)$$

The formation of magnesium hydroxide deposits (eq. 6) at the scribe is also taking place (anodic sites). The scribe that was initially clean with a metallic appearance becomes dark, as it can be seen in the inset images (Figs. 12c-h). While the most active anodic sites are located at the scribe due to the high surface area of the exposed metal, other anodic sites are present as well at other sites all across the surface [16]. They are formed underneath the coating at the metal/coating interface, which make their visibility only possible mostly upon blistering of the coating. However, after 12h of immersion time (Figs. 12c-h), these events are still not visible. This might be attributed to the reaction of magnesium hydroxide with the PEI (i.e. self-healing) at the metal/coating interface keeping the good adhesion of the coating to the substrate [18].

4. Conclusions

SiNC-PhPh/PEI coatings loaded with SiNC-PhPh particles worked as efficient pH-sensing and therefore color-signaling systems by spotting early corrosion events on AZ31. The change of PhPh color occurred upon outbreak of the local corrosion process and it can be seen by visual inspection. PEI coatings loaded with 5 wt.%. SiNC-PhPh particles offered optimal pH-sensing/color-signaling functionality. SiNC-PhPh particle agglomerate sized below 2.2 µm were homogenously dispersed in the polymer matrix.

Immersion tests have shown that the pH change for the system SiNC-PhPh/PEI coatings starts very fast and it is accompanied by the appearance of pink color from the PhPh and for that pH-values the self-healing process should start also. Especially, for dense coatings, color-signaling functionality succeeds to sense small corrosion events, while EIS testing failed to detect them. Dense transparent coatings performed better in color-signaling than the porous ones. DVIT assisted EIS tests have shown important clues for a fast color signaling matching the corrosion kinetics at the metal surface. Even the

smallest corrosion events were detected proving the high detection accuracy and resolution at micron range of the SiNC-PhPh particle agglomerates. Moreover, simulated drop atmospheric tests showed the high reproducibility of the sensing signal upon multiple uses.

Given the performance of these pH-sensing/color-signaling coatings, enhanced service life and reduction in maintenance costs could be achieved when combined with an appropriate inspection regime.

Acknowledgements

This work was supported by SMARCOAT European project (Marie Skłodowska-Curie grant agreement nº. 645662). Dr. S.V. Lamaka acknowledges the financial support of Alexander von Humboldt Foundation via Experienced Researcher Grant.

References

[1]. G.L. Song, A. Atrens, Corrosion Mechanisms of Magnesium Alloys, Advanced Engineering Materials, 1 (1999) 11-33.

[2]. G. Edward, W. Dietzel, K.U. Kainer, General and Localized Corrosion of Magnesium Alloys: A Critical Review, Journal of Materials Engineering and Performance, 22 (2013) 2875-2891.

[3]. R.-G. Hu, S. Zhang, J.-F. Bu, C.-J. Lin, G.-L. Song, Recent progress in corrosion protection of magnesium alloys by organic coatings, Progress in Organic Coatings, 73 (2012) 129-141.

[4]. R.B. Figueira, C.J.R. Silva, E.V. Pereira, Organic–inorganic hybrid sol–gel coatings for metal corrosion protection: a review of recent progress, Journal of Coatings Technology and Research, 12 (2015) 1-35.

[5]. J.E. Gray, B. Luan, Protective coatings on magnesium and its alloys — a critical review, Journal of Alloys and Compounds, 336 (2002) 88-113.

[6]. M. Bobby Kannan, W. Dietzel, C. Blawert, A. Atrens, P. Lyon, Stress corrosion cracking of rare-earth containing magnesium alloys ZE41, QE22 and Elektron 21 (EV31A) compared with AZ80, Materials Science and Engineering: A, 480 (2008) 529-539.

[7]. R. Supplit, T. Koch, U. Schubert, Evaluation of the anti-corrosive effect of acid pickling and sol–gel coating on magnesium AZ31 alloy, Corrosion Science, 49 (2007) 3015-3023.

[8]. U.C. Nwaogu, C. Blawert, N. Scharnagl, W. Dietzel, K.U. Kainer, Effects of organic acid pickling on the corrosion resistance of magnesium alloy AZ31 sheet, Corrosion Science, 52 (2010) 2143-2154.

[9]. S. Pommiers, J. Frayret, A. Castetbon, M. Potin-Gautier, Alternative conversion coatings to chromate for the protection of magnesium alloys, Corrosion Science, 84 (2014) 135-146.

[10]. F. Brusciotti, D.V. Snihirova, H. Xue, M.F. Montemor, S.V. Lamaka, M.G.S. Ferreira, Hybrid epoxy–silane coatings for improved corrosion protection of Mg alloy, Corrosion Science, 67 (2013) 82-90.

[11]. S.V. Lamaka, M.F. Montemor, A.F. Galio, M.L. Zheludkevich, C. Trindade, L.F. Dick, M.G.S. Ferreira, Novel hybrid sol–gel coatings for corrosion protection of AZ31B magnesium alloy, Electrochimica Acta, 53 (2008) 4773-4783.

[12]. S.V. Lamaka, G. Knörnschild, D.V. Snihirova, M.G. Taryba, M.L. Zheludkevich, M.G.S. Ferreira, Complex anticorrosion coating for ZK30 magnesium alloy, Electrochimica Acta, 55 (2009) 131-141.

[13]. D. Wang, G.P. Bierwagen, Sol–gel coatings on metals for corrosion protection, Progress in Organic Coatings, 64 (2009) 327-338.

[14]. S.V. Lamaka, H.B. Xue, N.N.A.H. Meis, A.C.C. Esteves, M.G.S. Ferreira, Fault-tolerant hybrid epoxy-silane coating for corrosion protection of magnesium alloy AZ31, Progress in Organic Coatings, 80 (2015) 98-105.

[15]. N. Scharnagl, C. Blawert, W. Dietzel, Corrosion protection of magnesium alloy AZ31 by coating with poly(ether imides) (PEI), Surface and Coatings Technology, 203 (2009) 1423-1428.

[16]. S.V. Lamaka, O.V. Karavai, A.C. Bastos, M.L. Zheludkevich, M.G.S. Ferreira, Monitoring local spatial distribution of Mg2+, pH and ionic currents, Electrochemistry Communications, 10 (2008) 259-262.

[17]. O.V. Karavai, A.C. Bastos, M.L. Zheludkevich, M.G. Taryba, S.V. Lamaka, M.G.S. Ferreira, Localized electrochemical study of corrosion inhibition in microdefects on coated AZ31 magnesium alloy, Electrochimica Acta, 55 (2010) 5401-5406.

[18]. T.F. da Conceicao, N. Scharnagl, W. Dietzel, K.U. Kainer, On the degradation mechanism of corrosion protective poly(ether imide) coatings on magnesium AZ31 alloy, Corrosion Science, 52 (2010) 3155-3157.

[19]. A. Zomorodian, M.P. Garcia, T. Moura e Silva, J.C.S. Fernandes, M.H. Fernandes, M.F. Montemor, Corrosion resistance of a composite polymeric coating applied on biodegradable AZ31 magnesium alloy, Acta Biomaterialia, 9 (2013) 8660-8670.

[20]. T.F. da Conceicao, N. Scharnagl, W. Dietzel, K.U. Kainer, Corrosion protection of magnesium AZ31 alloy using poly(ether imide) [PEI] coatings prepared by the dip coating method: Influence of solvent and substrate pre-treatment, Corrosion Science, 53 (2011) 338-346.

[21]. T.F. Conceicao, N. Scharnagl, C. Blawert, W. Dietzel, K.U. Kainer, Corrosion protection of magnesium alloy AZ31 sheets by spin coating process with poly(ether imide) [PEI], Corrosion Science, 52 (2010) 2066-2079.

[22]. N. Scharnagl, Blawert, C. , Coating of a magnesium component with polyetherimide solution, 2009, GKSS-Forschungszentrum Geesthacht G.m.b.H., Germany.US20090202849A1

[23]. K.V. Peinemann, J.F. Maggioni, S.P. Nunes, Poly(ether imide) membranes obtained from solution in cosolvent mixtures, Polymer, 39 (1998) 3411-3416.

[24]. R. Anne, M. Paul, D. Claude, C. Hubert, D. André, Poly(ether imide) membrane formation by water vapour induced phase inversion, Macromolecular Symposia, 188 (2002) 37-48.

[25]. F. Maia, J. Tedim, A.C. Bastos, M.G.S. Ferreira, M.L. Zheludkevich, Nanocontainer-based corrosion sensing coating, Nanotechnology, 24 (2013) 415502.

[26]. F. Maia, J. Tedim, A.C. Bastos, M.G.S. Ferreira, M.L. Zheludkevich, Active sensing coating for early detection of corrosion processes, RSC Advances, 4 (2014) 17780-17786.

[27]. J. Zhang, G.S. Frankel, Corrosion-Sensing Behavior of an Acrylic-Based Coating System, CORROSION, 55 (1999) 957-967.

[28]. I.M. El-Nahhal, S.M. Zourab, N.M. El-Ashgar, Encapsulation of Phenolphthalein pH-Indicator into a Sol-Gel Matrix, Journal of Dispersion Science and Technology, 22 (2001) 583-590.

[29]. V. Volovšek, K. Furić, L. Bistričić, M. Leskovac, Micro Raman Spectroscopy of Silica Nanoparticles Treated with Aminopropylsilanetriol, Macromolecular Symposia, 265 (2008) 178-182.

[30]. B.J. Briscoe, B.H. Stuart, S. Rostami, A Fourier transform Raman spectroscopy study of the crystallization behaviour of poly (ether ether ketone)/poly (ether imide) blends, Spectrochimica Acta Part A: Molecular Spectroscopy, 49 (1993) 753-758.

[31]. H.S. Isaacs, Y.M. Looi, J.H.W. de Wit, Behavior of laser welded steel in chloride solution studied using difference imaging, Corrosion Science, 49 (2007) 53-62.

[32]. H. Krawiec, S. Stanek, V. Vignal, J. Lelito, J.S. Suchy, The use of microcapillary techniques to study the corrosion resistance of AZ91 magnesium alloy at the microscale, Corrosion Science, 53 (2011) 3108-3113.

[33]. H.T. Ham, Y.S. Choi, I.J. Chung, An explanation of dispersion states of single-walled carbon nanotubes in solvents and aqueous surfactant solutions using solubility parameters, Journal of Colloid and Interface Science, 286 (2005) 216-223.

[34]. K. Gong, Q. Fang, S. Gu, S.F.Y. Li, Y. Yan, Nonaqueous redox-flow batteries: organic solvents, supporting electrolytes, and redox pairs, Energy & Environmental Science, 8 (2015) 3515-3530.

[35]. F. Maia, J. Tedim, A.D. Lisenkov, A.N. Salak, M.L. Zheludkevich, M.G.S. Ferreira, Silica nanocontainers for active corrosion protection, Nanoscale, 4 (2012) 1287-1298.

[36]. M. Pourbaix, Pergamon Press, London, 1966.

[37]. E. Ghali, W. Dietzel, K.-U. Kainer, General and localized corrosion of magnesium alloys: A critical review, Journal of Materials Engineering and Performance, 13 (2004) 7-23.

[38]. W. Albrecht, B. Seifert, T. Weigel, M. Schossig, A. Holländer, T. Groth, R. Hilke, Amination of Poly(ether imide) Membranes Using Di- and Multivalent Amines, Macromolecular Chemistry and Physics, 204 (2003) 510-521.

List of captions

Fig. 1 – SEM and Si elemental EDX mapping images, and respective particle size histogram plots of the 5 wt.% SiNC-PhPh/PEI films obtained by (a-c) protocol 1, (d-f) protocol 2 and (g-j) protocol 3.

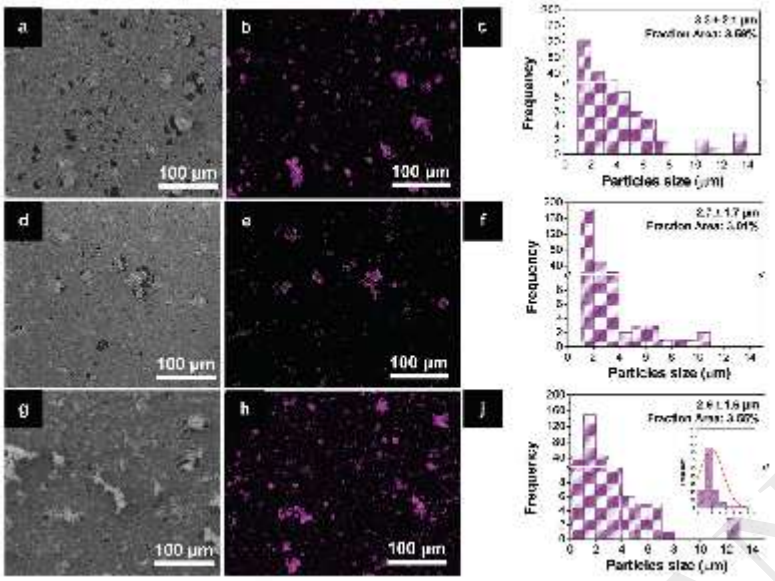

Fig. 2 – Si-elemental EDX mapping images of the SiNC-PhPh/PEI films for different SiNC-PhPh contents, and respective optical images of the films after 5 min of exposition to a drop of 0.05 M NaOH.

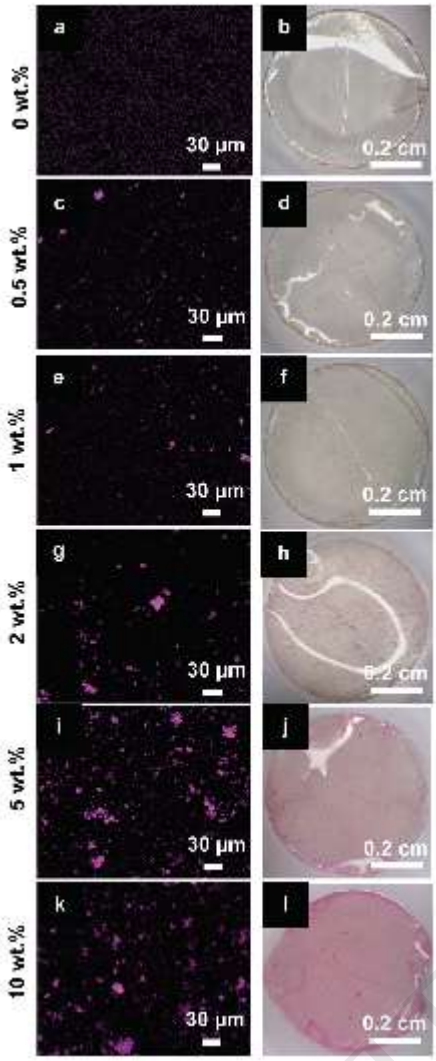

Fig. 3 – Dependence of the (a) SiNC-PhPh particle size and SiNC-PhPh particle area, and (b) particle content (vol.%) and particle fraction area on the particle content (wt.%) in the PEI films.

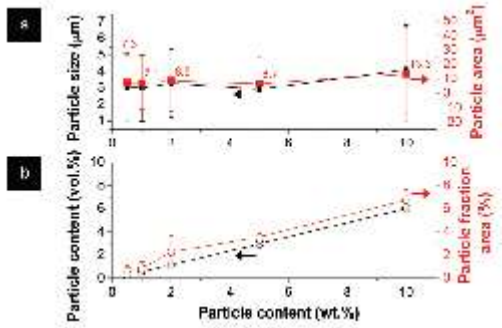

Fig. 4 – (a) Optical photographs recording of the color changes of the 5 wt.% SiNC-PhPh film sample in 0.05 M NaOH over time. (b) Cyclic test of color change at the same conditions of (a).

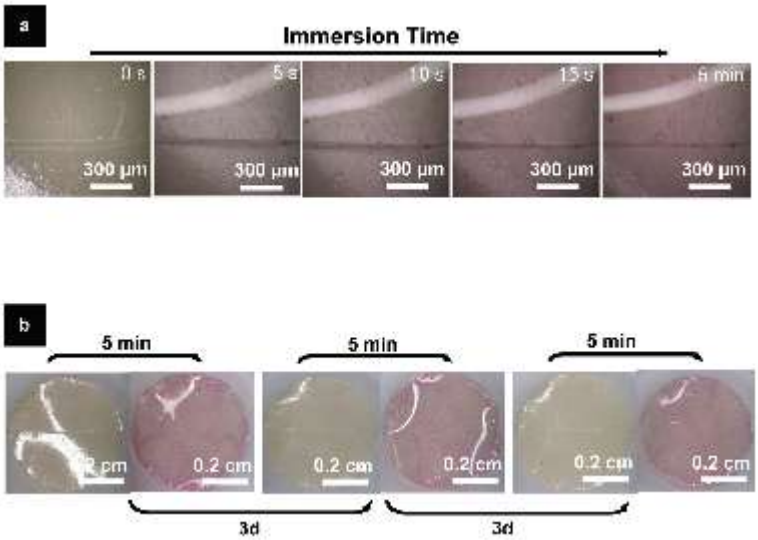

Fig. 5 – Optical photographs, SEM (top and cross-sectional views) and EDX mapping images, and respective particle size histogram plots of 5 wt.% SiNC-PhPh/PEI dip coated AZ31 substrates: (a-e) porous; (f-j) dense.

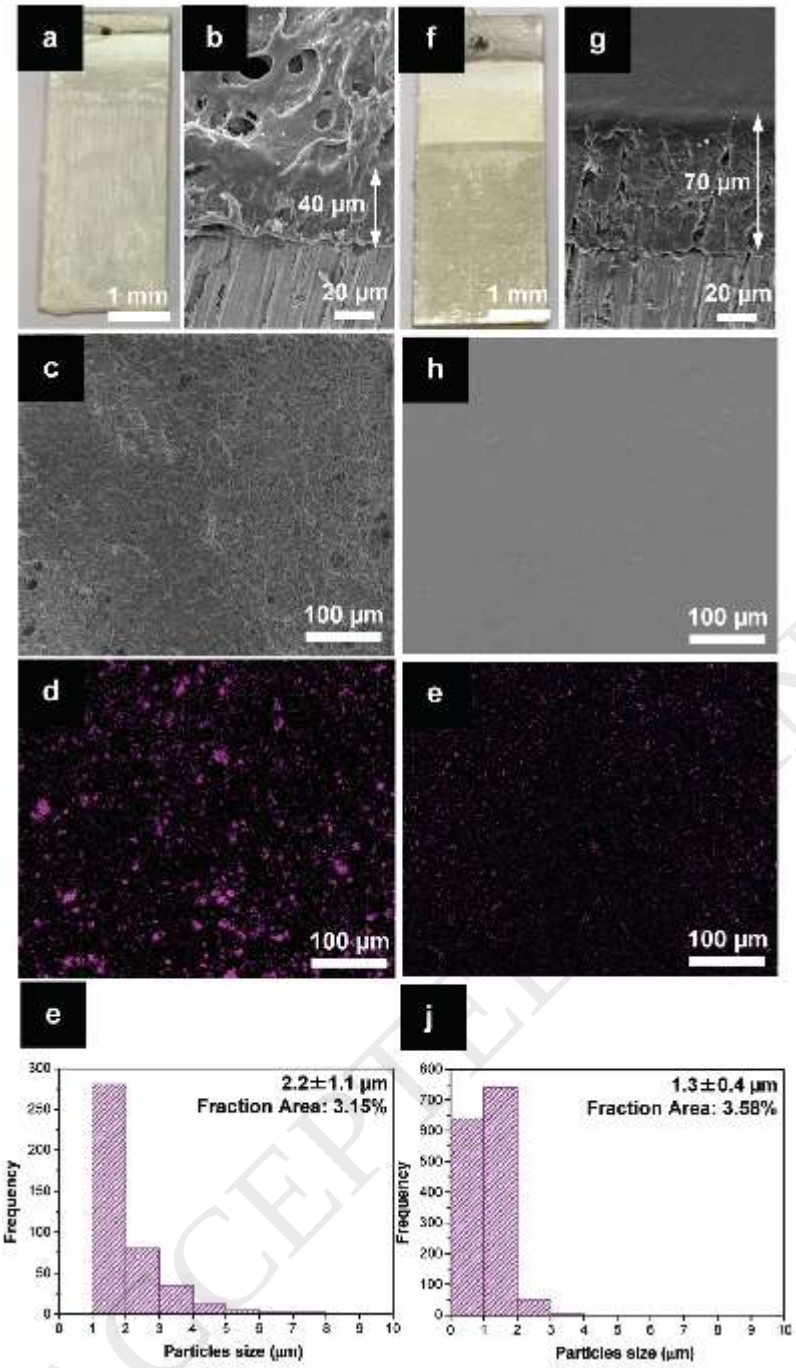

Fig. 6 – (a) Raman spectra of the SiNC-PhPh, dense PEI coatings and dense 5 wt.% SiNC-PhPh/PEI coatings. (b) Raman spectrum of the 5 wt.% SiNC-PhPh/PEI coating in the spectrum region highlighted in (a).

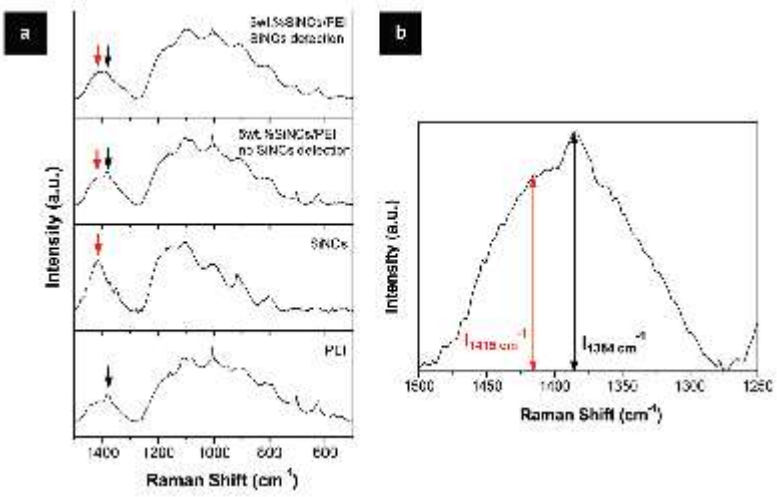

Fig. 7 – Confocal Raman mapping analyses of the dense 5 wt.% SiNC-PhPh/PEI coating: (a) photograph of the sample surface, (b) respective top-view image of the 3D reconstruction built from the Raman shift of SiNC-PhPh obtained in (a), and (c) tilted perspective of the 3D reconstruction of (b).

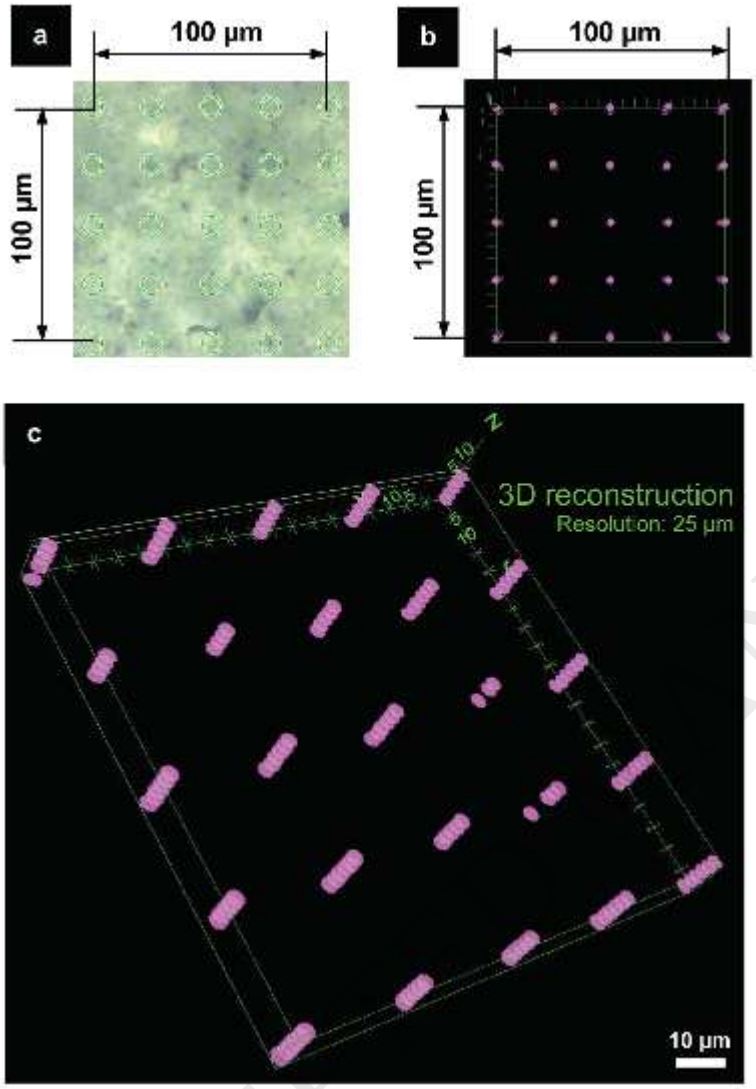

Fig. 8 – Evolution of the visual appearance during the immersion tests of PEI (control) and 5 wt.% SiNC-PhPh/PEI dip coated AZ31 substrates in 0.5 M NaCl: (a) porous (DMAc) and (b) dense (DCM) coatings.

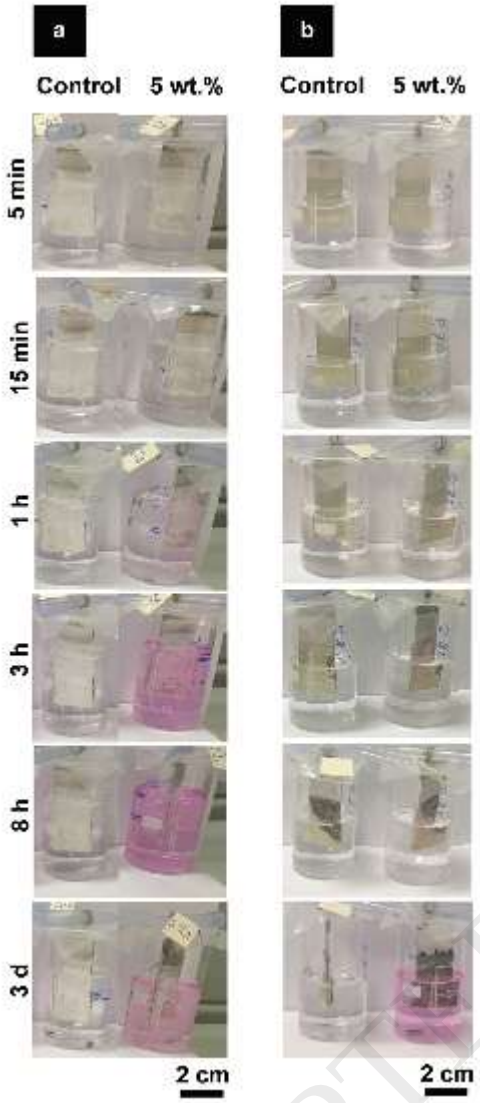

Fig. 9 – Magnified photographs of the color changes of the 5 wt.% SiNC-PhPh/PEI coatings in 0.5 M NaCl solution: (a) porous (DMAc) and (b) dense (DCM) coatings. Pink highlighted circles: color of PhPh detected.

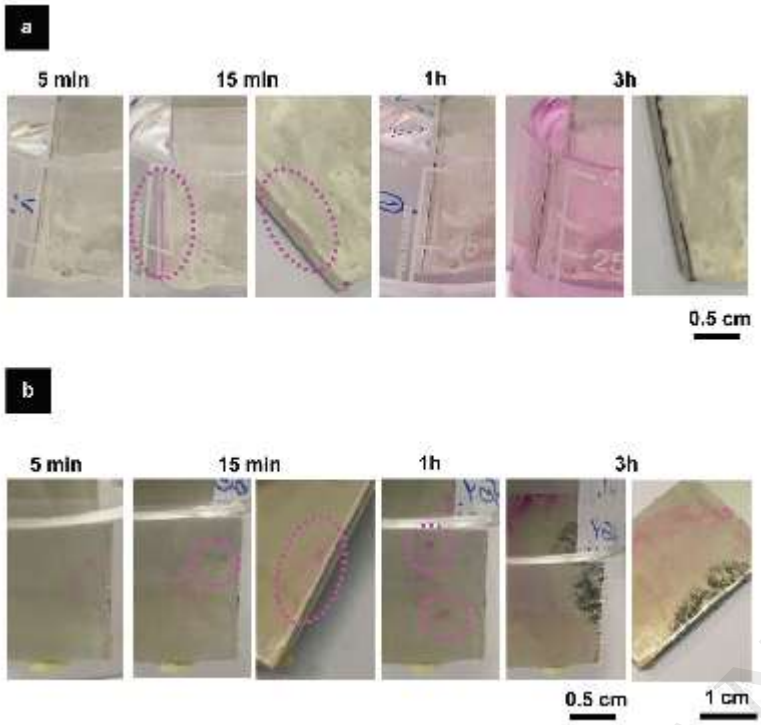

Fig. 10 – Bode plots of the AZ31 substrates coated with 5 wt.% SiNC-PhPh/PEI coatings after up to 24 hours immersion in 0.5 M NaCl solution: (a) porous (DMAc) and (b) dense (DCM) coatings.

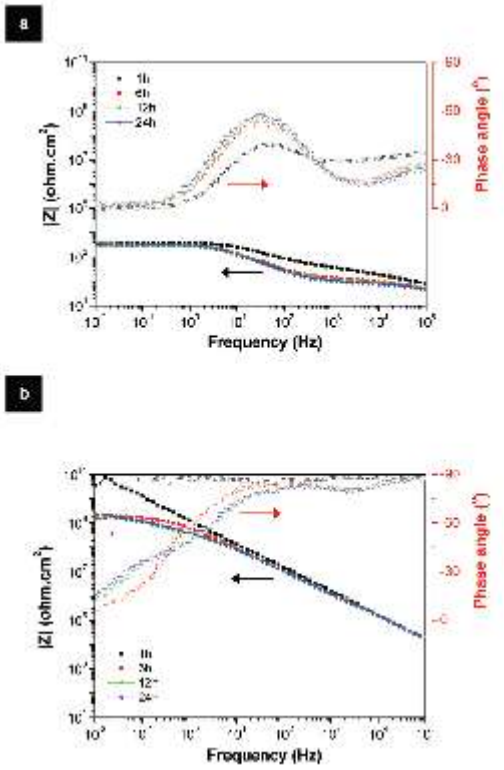

Fig. 11 – DVIT images and respective EIS (10^{-2} Hz) recording of (a and b) porous and (c and d) dense 5 wt.% SiNC-PhPh/PEI coated AZ31 substrates in 0.5 M NaCl over time.

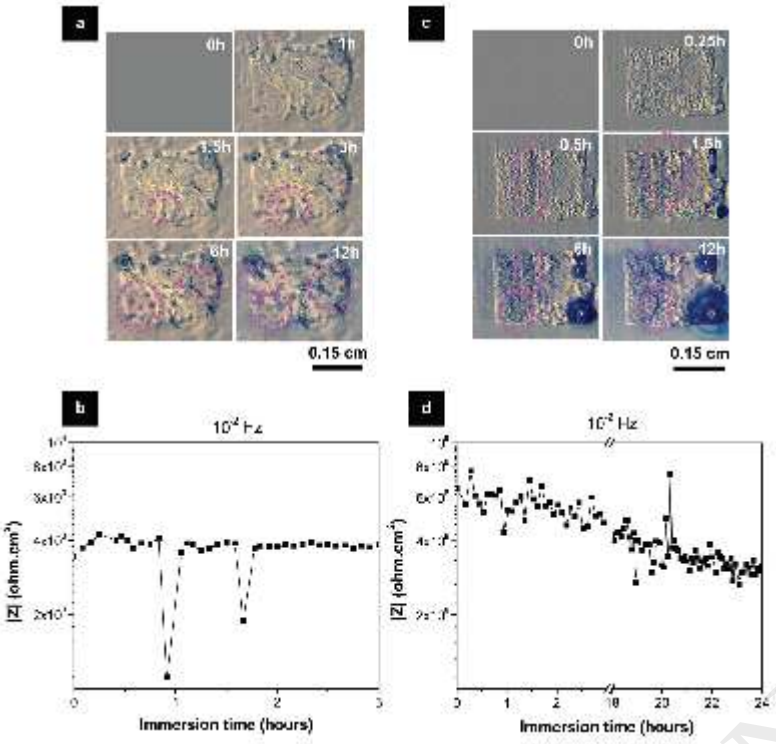

Fig. 12 – Optical and DVIT images recording of the dense 5 wt.% SiNC-PhPh/PEI coated AZ31 substrates with an artificial defect, after (a and b) 0 hours, (c and d) 0.08 hours, (e and f) 1 hour and (g and h) 12 hours in 0.5 M NaCl. Inset: images of the scribe for each time recorded.

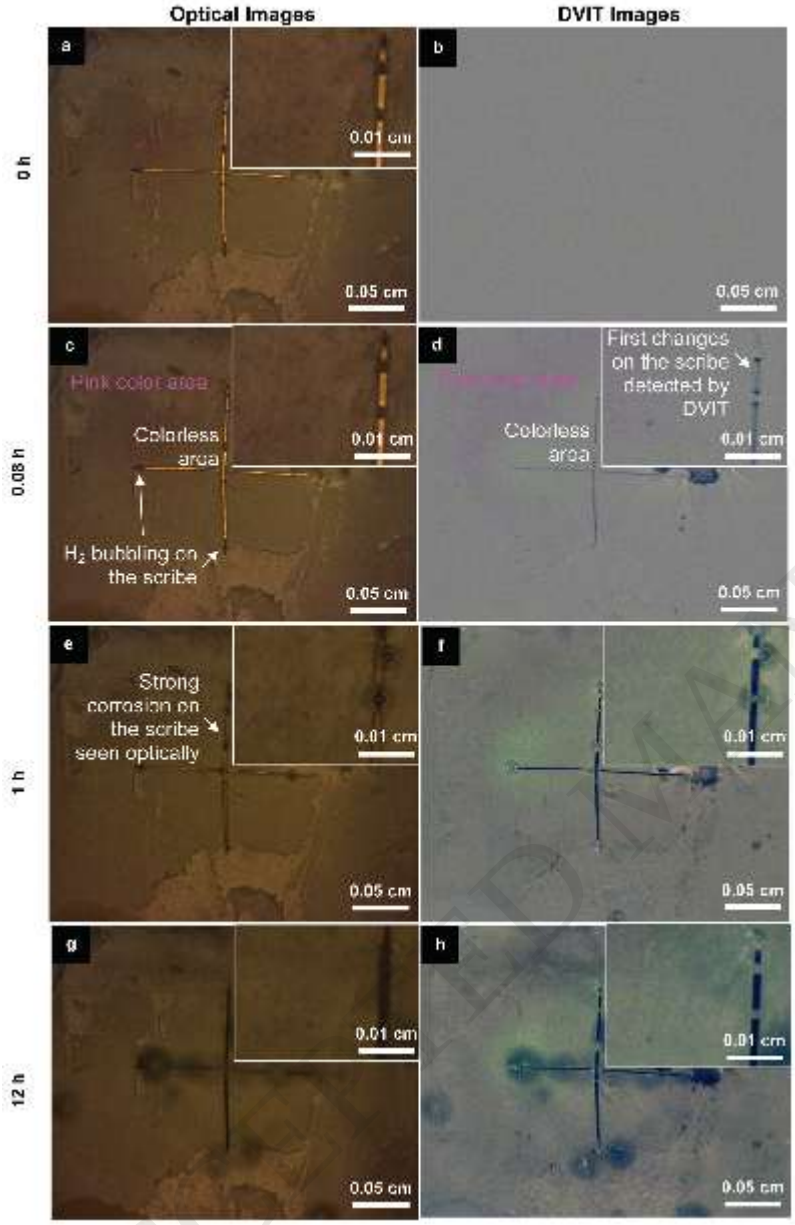

Table 1 – Coatings preparation conditions and SiNC-PhPh particle sizes in the final coatings.

Formulation	Formulation protocol steps	Porous coatings[a] SiNCs content (wt.%)	Dense coatings[b] SiNCs content (wt.%)	Coating process	SiNCs particle size (µm) porous | dense coatings
A	powders directly added to PEI solution (stirred, 800 rpm/1h)	0	-	bar-coating	-
		5		"	3.3 ± 2.1
B	1. powders predispersed in solvent (stirred, 650 rpm/1h) 2. stirred in PEI solution (800 rpm/1h)	0	-	bar-coating	-
		5		"	2.7 ± 1.7
C	1. powders predispersed in solvent (stirred, 550 rpm/5h) 2. stirred in PEI solution (300 rpm/24h)	0	0	bar[c]- and dip[d]-coating	-
		0.5	-	bar-coating	3.1 ± 2.1
		1	-	"	3 ± 2
		2	-	"	3.3 ± 2
		5[d]	5[d]	bar[c]- and dip[d]-coating	2.2 ± 1.1[d] | 1.3 ± 0.4[d]
		10	-	bar-coating	4.1 ± 2.7

[a] N,N'-Dimethylacetamide (DMAc)
[b] Dichloromethane (DMC)
[c] bar-coating, glass substrates
[d] bar-coating, metal substrates